Life Sciences in Space Research 5 (2015) 6–12

Contents lists available at ScienceDirect

Life Sciences in Space Research

www.elsevier.com/locate/lssr

Measurements of the neutron spectrum in transit to Mars on the Mars Science Laboratory

J. Köhler [a,*], B. Ehresmann [b], C. Zeitlin [f], R.F. Wimmer-Schweingruber [a], D.M. Hassler [b], G. Reitz [c], D.E. Brinza [e], J. Appel [a], S. Böttcher [a], E. Böhm [a], S. Burmeister [a], J. Guo [a], H. Lohf [a], C. Martin [a], A. Posner [d], S. Rafkin [b]

[a] Institute of Experimental and Applied Physics, Christian-Albrechts-University, Kiel, Germany
[b] Southwest Research Institute, Space Science and Engineering Division, Boulder, USA
[c] Aerospace Medicine, Deutsches Zentrum für Luft- und Raumfahrt, Köln, Germany
[d] NASA Headquarters, Science Mission Directorate, Washington DC, USA
[e] Jet Propulsion Laboratory, California Institute of Technology, Pasadena, CA, USA
[f] Southwest Research Institute, Earth, Oceans & Space Department, Durham, NH, USA

ARTICLE INFO

Article history:
Received 16 February 2015
Received in revised form 16 March 2015
Accepted 19 March 2015

Keywords:
Space radiation
Mars mission
Neutron dose rate
Neutron spectrum

ABSTRACT

The Mars Science Laboratory spacecraft, containing the Curiosity rover, was launched to Mars on 26 November 2011. Although designed for measuring the radiation on the surface of Mars, the Radiation Assessment Detector (RAD) measured the radiation environment inside the spacecraft during most of the 253-day, 560-million-kilometer cruise to Mars. An important factor for determining the biological impact of the radiation environment inside the spacecraft is the specific contribution of neutrons with their high biological effectiveness. We apply an inversion method (based on a maximum-likelihood estimation) to calculate the neutron and gamma spectra from the RAD neutral particle measurements. The measured neutron spectrum (12–436 MeV) translates into a radiation dose rate of 3.8 ± 1.2 μGy/day and a dose equivalent of 19 ± 5 μSv/day. Extrapolating the measured spectrum (0.1–1000 MeV), we find that the total neutron-induced dose rate is 6 ± 2 μGy/day and the dose equivalent rate is 30 ± 10 μSv/day. For a 360 day round-trip from Earth to Mars with comparable shielding, this translates into a neutron induced dose equivalent of about 11 ± 4 mSv.

1. Introduction

The Mars Science Laboratory (MSL) mission was launched on November 26, 2011 and landed on Mars on August 6, 2012 after a 253-day cruise. On board the rover Curiosity is the Radiation Assessment Detector (RAD) which has been designed to "fully characterize the Martian radiation environment" (Hassler et al., 2012). However, the cruise to Mars was a unique opportunity to measure the radiation environment inside a spacecraft for future manned missions to Mars. Therefore RAD was operated during most of the cruise from Earth to Mars, gathering the first science data of Curiosity's mission. With the exception of some short interruptions, RAD provided a continuous radiation measurement from inside the spacecraft. RAD was initially operated on an 8-minute observation cadence, with a 100% duty cycle; as the distance between the spacecraft and Earth increased, it was necessary to reduce data volume, so that the cadence was increased to 16 minutes in late January 2012. The typical duty cycle from that time forward was 50%. Radiation dose, dose equivalent and linear energy transfer spectra inside the MSL spacecraft on its trip to Mars have been presented in Zeitlin et al. (2013).

The innovative design of RAD allows us to measure charged particles as well as gamma rays and neutrons. Obtaining charged particle spectra is fairly straightforward (Hassler et al., 2012; Ehresmann et al., 2014), but the multiple interaction processes of neutral particles result in a complex instrument response to neutral particles, which does not allow a similarly straightforward interpretation of neutral particle spectra. Measured neutral particle spectra do not give a direct picture of the real neutron and gamma spectra. Instead, a complex inversion method is required for their interpretation, as was presented in Köhler et al. (2014) for neutral particle measurements on the Martian surface. In this work we present the corresponding gamma ray and neutron measurements and spectra as they were present in the spacecraft during MSL's cruise phase.

* Corresponding author.
E-mail address: koehler@physik.uni-kiel.de (J. Köhler).

http://dx.doi.org/10.1016/j.lssr.2015.03.001
2214-5524/

1.1. Motivation for measuring gamma and neutron spectra

For a manned mission to Mars, a large fraction of the radiation will be incurred during the cruise to and back from Mars (Zeitlin et al., 2013; Hassler et al., 2014). For instance, a 180 day one-way trip would result in a dose equivalent of 0.33 Sv. This is approximately 30% of the total expected dose rate for a return mission to Mars, consisting of a 180 day cruise to Mars, a 500-day surface stay and a 180-day return transit.

The contributions to the radiation environment inside the spacecraft are complex: primary Galactic Cosmic Rays (GCR) and Solar Energetic Particles (SEP) may pass through the spacecraft to deliver dose directly, or they may interact with the spacecraft material to produce secondary particles. As a result of the secondary particle production, there are more types of particles which form the radiation environment inside a spacecraft than outside, and neutrons are among those of greatest concern from the perspective of radiation protection. Interactions of GCR ions produce neutrons over a broad energy range from eV to GeV (Hess et al., 1959). Over most of that range, the biological damage associated with a given fluence of neutrons (expressed as dose equivalent per unit fluence) is modest, comparable to or less than that caused by the same fluence of charged particles. But neutron fluences increase with shielding depth and can be quite large. The fractional contribution of neutrons to dose equivalent increases with shielding depth (Simonsen et al., 2000), as charged particles either range out or undergo nuclear interactions. At large depths, such as in a habitat buried a few meters below the Martian surface, the neutron contribution may approach 50%. Furthermore, biological effects of neutron exposure are highly uncertain (Durante and Cucinotta, 2011), especially high above the fission energies and the 14-MeV Deuterium–Tritium energy where most neutron radiobiology experiments have been conducted. The neutron radiation inside the spacecraft is almost completely generated as secondary particles of GCR spacecraft interaction. Because of the finite lifetime of neutrons there is only a very low flux of solar neutrons at 1 AU (Feldman et al., 2010; Share et al., 2011). To our knowledge, this work presents one of the few high-energy neutron measurements in space.

1.2. The MSL spacecraft

The RAD instrument is mounted beneath the top deck of the rover Curiosity, which was inside the MSL spacecraft on its trip to Mars. Curiosity was located beneath the descent stage and above the heat shield, which provide additional shielding against the deep space radiation environment. Because secondary particles are produced in the shielding, knowledge thereof is crucial for estimating the contribution of neutral particles to the cruise radiation environment. A simplified model of the shielding of the upper hemisphere around RAD was created by Shawn King at the Jet Propulsion Laboratory, as shown in Fig. 1. Note that shielding values for polar angles above 40 degrees are considered to be approximations, because the simplified model focuses on the upward directed field of view pertinent to charged particle measurements. Most of the solid angle is merely lightly shielded (areal density < 10 g/cm^2), the remaining solid angle is shielded with varying depth, with up to 90 g/cm^2 for particle trajectories through a fuel tank filled with hydrazine. The lower hemisphere, which is not shown in Fig. 1, is much more uniform and dominated by the RAD electronic box (8 gm/cm^2) and the spacecraft heat shield (1.5 g/cm^2) (Zeitlin et al., 2013). Although a spacecraft designed for a human crew would most likely be designed to have a more homogeneous distribution of shielding with few lightly-shielded areas, the crew would be exposed to a similar composition of neutral particles, since those are produced in the shielding itself.

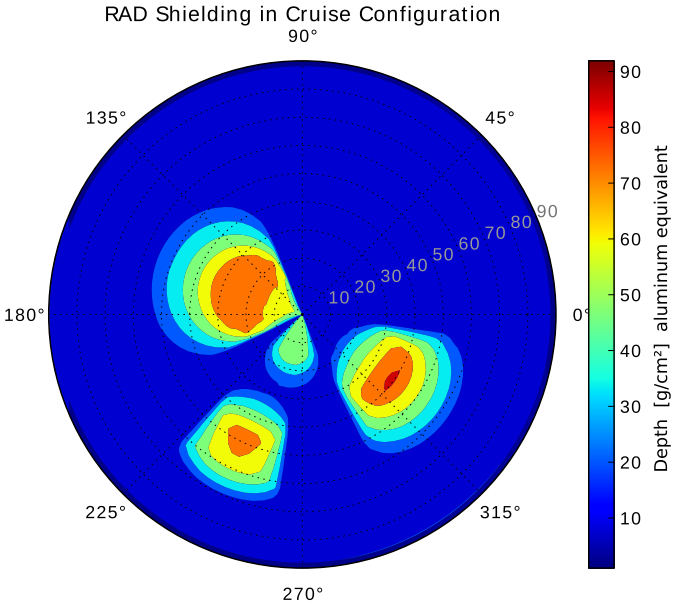

Fig. 1. Approximate representation of the shielding distribution. The center corresponds to the field of view direction of the RAD charged particle telescope, which was looking towards the sun during most of the cruise phase. Shielding depths are given in g cm^{-2} of aluminum equivalent shielding depth. Note that shielding values for polar angles above 40 degree are merely approximations, because the simplified model focuses on the upward directed field of view.

The available information is far from sufficient to create a detailed simulation of the gamma and neutron production through GCR spacecraft interaction. E.g., the exact composition of the shielding and the position of different elements such as the hydrazine tanks or the parachute are not known to us. Therefore, we can not attempt a quantitative simulation of the GCR induced neutron and gamma spectra, but rather a simulation to estimate the expected shapes of the gamma and neutron spectra induced by the interaction of GCR on aluminum and GCR on hydrazine.

2. Neutral particle measurements with RAD

The RAD instrument houses several detectors for charged and neutral particle measurement. Charged particles are measured by three silicon detectors (A, B, C), followed by a Tl-doped cesium iodide scintillator (D), neutral particles are measured by the combination of D and a plastic scintillator (E). The D scintillator is highly sensitive to gamma rays, the E detector is highly sensitive to neutrons. Both scintillators are enclosed by an anticoincidence (C, F) to reject charged particles. A detailed overview is given in Hassler et al. (2012), Fig. 2 shows a schematic view of the instrument. Each event is analyzed via pulse-height analysis on board. The events are classified according to a priority scheme and only a subset of the measured events is sent back to Earth together with scaling factors. The scaling factors can be used to reconstruct the measurement (Hassler et al., 2012).

2.1. Mathematical background

As explained in Köhler et al. (2014), the charged particles that are stopped by the scintillators in RAD deposit their full energy. In contrast, neutral particles do not necessarily stop in either detector and can create an energy deposit which is randomly distributed, ranging from zero up to their incident energy. This makes the measurement of neutral particle spectra very difficult. Further problems arise from the fact that the D detector is not only sensitive to gamma rays, but also to neutrons, albeit to a lesser degree.

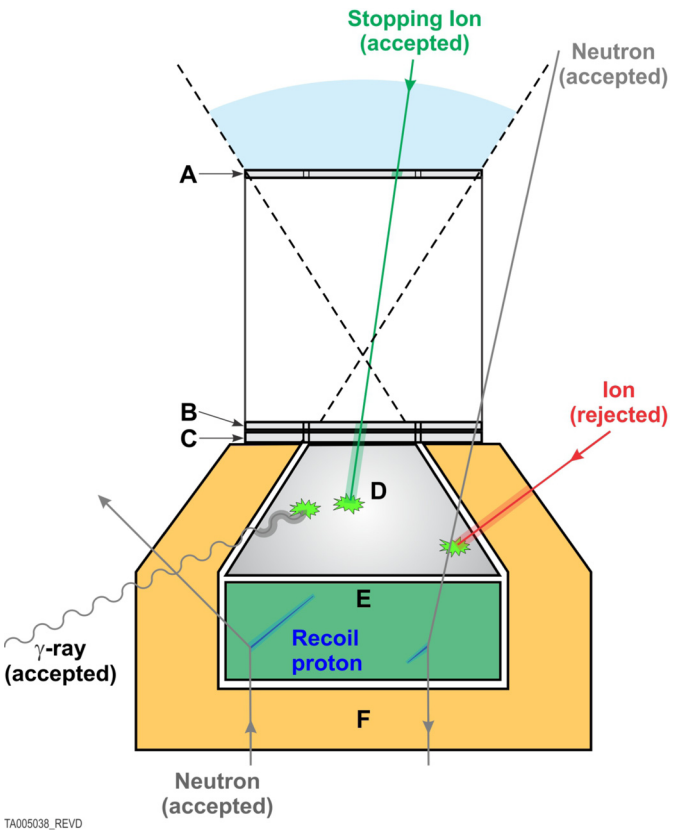

Fig. 2. Schematic view of the RAD instrument, consisting of three silicon detectors (A, B, C), a caesium iodide scintillator (D) and a plastic scintillator (E). Both scintillators are surrounded by a plastic anticoincidence (F). For detecting charged particles, A, B, C, D, E are used as a telescope. The hexagonal shaped E detector has a diameter of 4.7 cm and a height of 1.8 cm. The height of the D detector is 2.8 cm. Neutral particles are detected in D and E using C and F as anticoincidence. During cruise the viewing direction of the telescope is directed towards the sun. Figure from Köhler et al. (2014).

Similarly, E is also sensitive to gamma rays. Therefore, the neutral particle measurements in D and E do not simply reflect the incident gamma and neutron spectra, respectively. In Köhler et al. (2011), Köhler (2012), Köhler et al. (2014) we demonstrated that the incident gamma/neutron spectra must instead be obtained via an inversion method. For the inversion, the measurements of D and E are processed as histograms $\vec{z}_D$ and $\vec{z}_E$, where the vector element $z_{D/E,i}$ is the number of counts in the i-th energy bin of the histogram of the energy distribution in D/E. The spectra of the incoming particles are also described as vectors $\vec{f}_{\gamma/n}$, where $f_{\gamma/n,i}$ is the gamma-ray/neutron intensity at energy bin E_i. A measurement can now be described by

$$\vec{z}_{D/E} = \mathbf{A}_{D/E,\gamma/n} \cdot \vec{f}_{\gamma/n}, \tag{1}$$

where $\mathbf{A}_{D/E,\gamma/N}$ is an $l \times k$ matrix which describes the response of D/E to gamma rays/neutrons. Defining

$$\vec{z} = (z_{D,1}..., z_{D,k}, z_{E,1}, \ldots z_{E,k}), \text{ and} \tag{2}$$

$$\vec{f} = (f_{\gamma,1}..., f_{,\gamma,l}, f_{n,1}, \ldots f_{n,l}). \tag{3}$$

Eq. (1) can be expressed as a single equation for gamma rays and neutrons in D and E

$$\vec{z} = \mathbf{A} \cdot \vec{f}, \tag{4}$$

where the matrix **A** describes the Detector Response Function (DRF) consisting of

$$\mathbf{A} = \begin{pmatrix} \mathbf{A}_{D,\gamma} & \mathbf{A}_{D,n} \\ \mathbf{A}_{E,\gamma} & \mathbf{A}_{E,n} \end{pmatrix}. \tag{5}$$

In principle Eq. (4) can be solved for $\vec{f}$ by obtaining A^{-1}. However, this is rarely possible since the measurement contains statistical errors, which then can lead to unphysical results for $\vec{f}$, such as negative count rates. Eq. (4) can be formulated as a minimization problem with constraints

$$\min \sum_i \left(\frac{\sum_j A_{ij} f_j - z_i}{\sigma_i^2} \right)^2, \quad \text{with } f_i \geq 0, \tag{6}$$

where σ_i is the error for measurement z_i. In Köhler et al. (2011) a minimization function based on Poisson statistics was found to create the best results. However, since the MSL/RAD neutral particle measurements do not follow Poisson statistics exactly (see Section 2.2), we selected a minimization function based on Gaussian statistics, as done in Köhler et al. (2014).

The DRF used here, shown in Fig. 3, was obtained using the GEANT4 Monte Carlo code (Agostinelli et al., 2003).[1] The simulation is based on a detailed model of the instrument which includes effects such as electronic and optical noise in D, E, and F. A detailed description of the simulation setup and general approach can be found in Köhler et al. (2011), Köhler (2012). The fidelity of GEANT4 in describing the response of the detector to neutral particles correctly was verified in several calibration runs at Physikalisch-Technische Bundesanstalt and The Svedberg Laboratory (Hassler et al., 2012; Köhler et al., 2011). As in Köhler et al. (2014), we use QGSP_BERT_HP physics list to calculate the DRF. An additional DRF based on the QGSP_BIC_HP physics list was used to estimate the uncertainties due to the differences between the BINary and the BERTini intranuclear cascade model. To ensure a realistic behavior, the simulation includes instrument effects such as electronic behavior and optical noise (Köhler et al., 2011; Köhler, 2012).

For the measurements during cruise, the detection threshold for energy deposits in D is set to 15 MeV, and for E to 4 MeV. This is not caused by detector efficiency, but by the constraints of the onboard signal processing, which would be overwhelmed by particles from Curiosity's radioisotope thermoelectric generator if detection thresholds were reduced. To ensure a clean measurement, the neutral particle measurements consider only events above 20 MeV in D and above 10 MeV in E. The maximum energy in the D/E measurements were selected to be 400/300 MeV, which is well above any expected neutral particle energy deposit. In the following, we refer to energy depositions in units of MeV, with the scintillator light output calibrated to minimum-ionizing charge-one particles (sometimes denoted "MeVee" for MeV electron equivalent).

For the GEANT4 modeling, the energy range of the incident neutron/gamma spectra was selected to be 10–1000 MeV for gamma rays and 12–1000 MeV for neutrons. Minimum energies were selected in such a way that a significant fraction of gammas and neutrons, respectively, would create energy deposits above the measurement threshold in E. The maximum energy of 1000 MeV is a compromise between rapidly decreasing detection efficiency at higher energies and wanting to minimize the effect of particle energies which are beyond the inversion energy range but create energy deposits in the measured energy range, e.g. a 2 GeV neutron which created a 50 MeV energy deposit in E. Because of better statistics and a later fine tuning of the instrument's configuration,

[1] In contrast to Fig. 3, the DRF efficiency presented in Köhler et al. (2014) was not scaled with the energy range of the incoming spectrum, i.e. 995 MeV for gammas, and 992 MeV for neutrons. This leads to an apparent difference of three orders of magnitude.

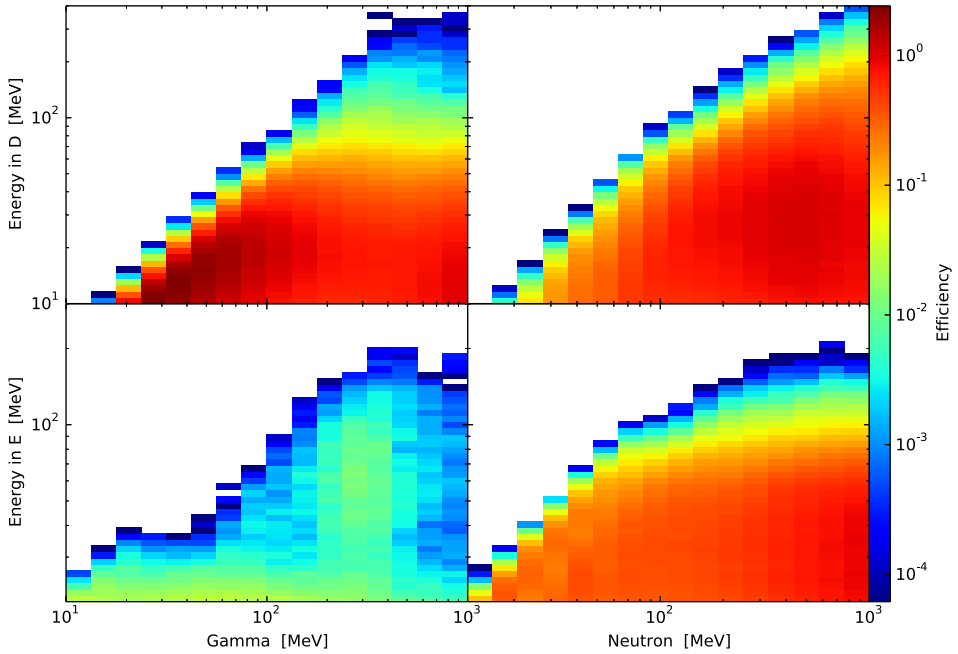

Fig. 3. The DRF for detecting gamma rays and neutrons with D, E. The x-axes show the energy of the incoming particles, the y-axes show the measured energy in D and E. The color denotes the efficiency [cm^2 MeV] for detecting a particle with a given energy in a certain measurement channel. I.e., the color coded values give the number of events in a certain measurement channel for an intensity of 1/(cm^2 MeV) of incoming particles with a given energy. The DRF shown here uses 96×32 bins, i.e. 16 bins for the gamma ray and neutron spectrum respectively.

the histogram energy ranges used in Köhler et al. (2014) extend to lower energies than the ones presented here for the cruise phase.

2.2. Neutral particle histograms of D and E

To obtain the neutral particle histograms for D and E, we select those events in D/E which do not create any signal in the surrounding anticoincidence (AC). The AC threshold is set to 20 keV for C and 0 keV for F. A threshold of 0 keV in F means, that only events where electronic noise creates a negative signal in F are accepted, i.e. exactly half of the valid events. This method is used because of the comparatively large noise in F, which means that energy deposits often cannot be identified clearly. This method has the advantage that the contamination of the measurement by charged particles is minimized.

Fig. 4 shows the combined neutral particle measurement for the following Day of Year periods in 2012: 30–66, 75–123, 124–136, 140–161, 163–199. These periods were selected to avoid contamination by high proton count rates during SEP events, and also to avoid effects from RAD configuration changes; they correspond to a total of 1385.8 hours of measurement.

As mentioned above, only a very small subset of neutral particle Pulse-Height Analysis (PHA) records is sent back to Earth. These are classified into different priorities and must be scaled accordingly to obtain the real number of events (Hassler et al., 2012). The neutral particle measurements contain events from four different priorities. For each priority, p, one histogram $\vec{z}_p$ is calculated and the corresponding errors, $\vec{\sigma}_p$, are estimated according to counting statistics. Each histogram is then scaled with the appropriate weighting factor, c_p. The resulting measurement is given by the sum of the weighted histograms

$$z_i = \sum_{p=0}^{3} c_p \cdot z_{i,p} \tag{7}$$

$$\sigma_i = \sum_{p=0}^{3} c_p \cdot \sqrt{\max(1, z_{i,p})}, \quad \text{where} \tag{8}$$

$$c_p = \frac{N_{\text{measured}}}{N_{\text{telemetered}}} \tag{9}$$

Although the measurements for one priority $z_{i,p}$ are based on Poisson statistics, the resulting weighted measurements z_i are no longer based on Poisson statistics. Note that the errors due to counting statistics in N_{measured} and $N_{\text{telemetered}}$ are neglected because they are small compared to $\sqrt{z_{i,p}}$.

3. Gamma/neutron spectra calculated with 16 bin energy resolution

In minimization problems the choice of the initial guess is often crucial for finding the global minimum (Köhler et al., 2014). To ensure that the inversion yields a minimum close to the global minimum, the inversion is repeated for a large set of initial guesses. From all inversion results the one with the smallest error value (Eq. (6)) is selected as the most likely result. Here the initial guesses are given by a set of power laws with spectral indices in a range of $0.8 < S_{\gamma/n} < 2$. To avoid unphysical jumps in the spectra we introduce an additional constraint, $0.5 < f_{i+1}/f_i < 100$, in Eq. (6). The last three bins of the gamma/neutron spectra are excluded from this constraint, to act as overflow bins for particles with an energy above 1 GeV. In Köhler et al. (2014) only the last bin was used as an overflow bin. However, since the cruise measurements are based on comparatively few counts and the detector response is nearly indistinguishable for different high energy particles (Fig. 3), it is necessary to use the last three bins for overflow. The errors were determined via a Bootstrap-Monte Carlo technique (Press, 2007) and represent the uncertainties due to the statistics of the measurement and the uncertainties introduced by the ill-posed nature of the inversion problem, but they do not represent the uncertainties in the DRF or the calibration. Therefore, the procedure described above was performed several times to include possible uncertainties due to the GEANT4 physics model or errors in the calibration. I.e., the inversion was repeated for DRFs based on the Bertini and Binary cascade model, and for different calibration values of ±10%. The deviation of those results are included in

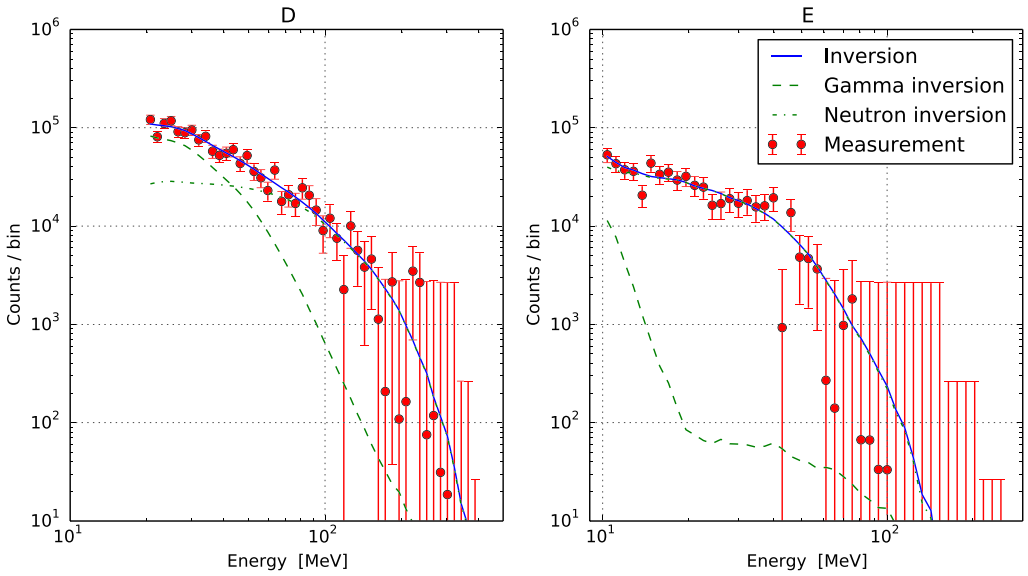

Fig. 4. Neutral particle measurements from the cruise to Mars (red) in the scintillators D (left) and E (right) and the result ($\mathbf{A}\cdot\vec{f}$) of inversion (blue). The individual contribution of gamma rays and neutrons ($\mathbf{A}\cdot\vec{f}_\gamma, \mathbf{A}\cdot\vec{f}_n$) is shown as a green dashed and green dashed–dotted line respectively. (For interpretation of the references to color in this figure legend, the reader is referred to the web version of this article.)

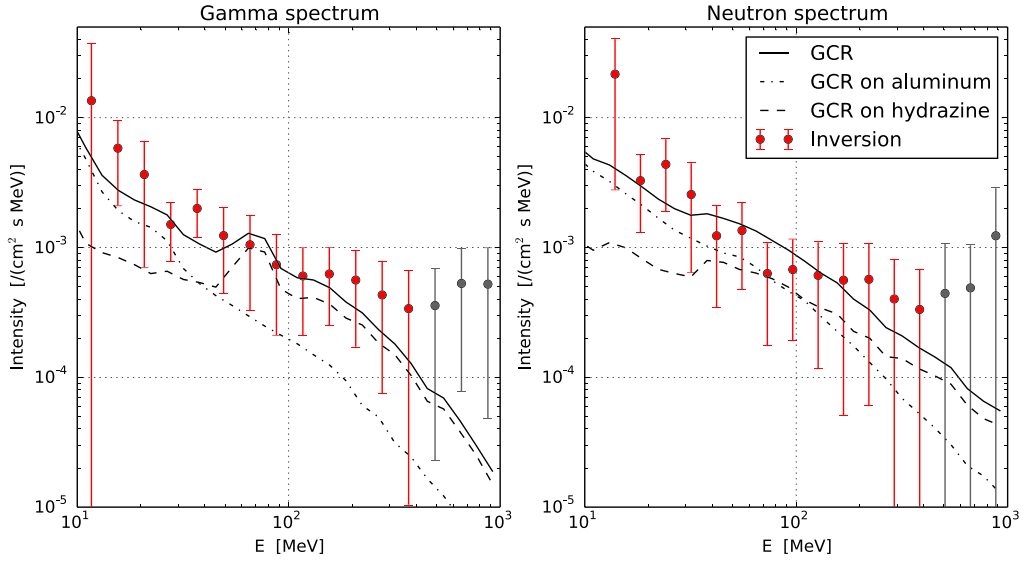

Fig. 5. Neutral particle spectra resulting from the inversion (red). Overflow bins are marked grey, and should not be interpreted as part of the inverted gamma or neutron spectrum. The black curve shows a qualitative estimation of the expected neutral particle spectra, resulting from GCR – aluminum and hydrazine interaction, calculated via GEANT4. (For interpretation of the references to color in this figure legend, the reader is referred to the web version of this article.)

the errors as well, however, the errors are dominated by the uncertainties due to the statistics of the measurement.

Fig. 5 shows the resulting inverted spectra, i.e., the particle spectra as they would be observed inside a similarly-shielded spacecraft on its way to Mars. The gamma spectrum is shown in the left panel and the neutron spectrum is shown in the right panel. The black curves show a qualitative estimation of the gamma and neuron spectra created by the spacecraft. Those spectra have been obtained with a GEANT4 simulation, where GCR proton and alpha spectra have been shot at a layer of aluminum and hydrazine, respectively. The main source of secondary neutrons are inelastic scattering of GCRs with aluminum and hydrazine. High energy gamma-rays are mainly generated via π^0 decays. The resulting neutron and gamma spectra were scaled in intensity to fit the inverted spectra. Because the exact geometry and composition of the spacecraft is not available to us, and the secondary particle spectra measured at RAD can depend significantly on the surrounding geometry, we did not attempt a quantitative calculation with a full featured model of the spacecraft. The reduced χ^2 of the inverted spectrum is 0.98 (compare Fig. 4, blue and red curve).

The gamma and neutron intensities above 40 MeV are likely due to GCR-hydrazine interactions, while the intensities below 40 MeV appear to be mainly generated by GCR-aluminum interactions. Curiosity's radioisotope thermoelectric generator emits a steady background of neutrons and gamma rays. These contributions were measured during ground tests and showed that there is no significant contribution of gammas and neutrons above 10 MeV in D or E.

Dose and dose equivalent for the neutron spectrum for the energies 12–436 MeV, can be calculated using the values provided in United States Nuclear Regulatory Comission (2009). Because the conversion values are only available for a sparse set of energies, the values are linearly interpolated and re binned to match the

calculated neutron spectrum. The dose equivalent can be obtained directly, the dose can be obtained by scaling the dose equivalent with the quality factor Q. Calculating dose and dose equivalent for the neutron spectrum for the energies 12–436 MeV, using United States Nuclear Regulatory Comission (2009), yields:

Dose equivalent rate: 19 ± 5 μSv/day

Dose rate: 3.8 ± 1.2 μGy/day

4. Discussion/conclusion

In this paper we used an inversion method to determine the gamma and neutron spectra measured inside the MSL spacecraft during the cruise from Earth to Mars. Since the primary source of gamma rays and neutrons is the interaction of the GCR with the spacecraft, the results were compared to GEANT4 simulations of GCR-aluminum and GCR-hydrazine interactions. The simulations, which were scaled in intensity to match the measurement, can explain the inversion results within the given errors.

At energies above 150 MeV, both the gamma and neutron spectrum show higher intensities than the GEANT4 simulation. Although this discrepancy is within the given error bars, it appears to be systematic and could be a real effect. One possible explanation is the low fidelity of the GEANT4 model, which does not include any spacecraft geometry, neglects spacecraft material other than aluminum and hydrazine and does not include GCR particles with $Z > 2$.

Another explanation for large intensities at high energies could be an inefficiency of the anticoincidence, which could falsely accept charged particles. While this effect would have little influence at lower energies, where the neutral count rate is high, it could have some influence at higher energies, where the neutral count rate is low.

To verify that the increased intensity is not just an effect of incorrect calibration values, a 10% error on the calibration was assumed and the inversion was tested for several different calibration values within this uncertainty. Further we tested DRFs which used Bertini and Binary cascade models, to verify that this effect does not depend on the used physics model. Although the effect does not depend on the used model or calibration, inaccuracies in the GEANT4 physics list as well as any unaccounted behavior of the RAD instrument cannot be completely excluded, especially since there is still a lack of neutron cross-section data for higher energies (Koning, 2007), and theoretical models, such as Bertini and Binary cascade, show different predictions for neutron cross-sections and production (Ivanchenko, 2004). Note that an increased intensity of high energy neutrons was also observed in Köhler et al. (2014).

Comparing the neutron induced dose with the values found by Zeitlin et al. (2013), shows that the neutrons (in the energy range 12–436 MeV) create only a small fraction of the total dose rate (3.8 μGy/day out of 480 μGy/day) and the total dose equivalent rate (19 μSv/day out of 1840 μSv/day). When comparing those values, one needs to take into account that the RAD dose rate measurement, as described in Zeitlin et al. (2013), contains all energy deposits above an energy threshold of 3 MeV. To get an estimate of the dose rate contribution from the "full" neutron spectrum, we calculate the dose rate for the GEANT4 simulation (black curve in Fig. 5) for all neutron energies above 0.1 MeV. A summary of the values is given in Table 1.

In principle the combined dose of neutrons and gammas in E could be calculated directly from the measurement shown in Fig. 4. However, high energy gammas and neutrons can create recoil particles that leave E and trigger the anti-coincidence F. Those events are not contained in the neutral particle histogram; we therefore expect that a direct calculation based on the E energy deposit spectrum would underestimate the dose rate. A straightforward analysis confirms this. Although this underestimation creates some uncertainty, Fig. 4 clearly shows, that in the observed energy range, the neutrons account for almost the complete neutral particle dose in E.

Table 1
Dose rate and dose equivalent rate for the calculated neutron spectrum. The measurement covers an energy range of 12–436 MeV, the simulation extends this range to 0.1–1000 MeV.

	Measurement	Simulation
Dose equivalent rate	19 ± 5 μSv/day	30 ± 10 μSv/day
Dose rate	3.8 ± 1.2 μGy/day	6 ± 2 μGy/day

Drake et al. (2010) state a value of 180 days for a reference manned mission to Mars. For a round-trip from Earth to Mars with comparable shielding, the dose values above translate into a dose equivalent of 11±4 mSv, compared to 660 mSv for all particle species. More typical round-trip times are ~500 days, based on the Hohmann minimum energy solution as first described in Hohmann (1994). Folta et al. (2012) describes an option to minimize the duration of the round trip using on-orbit staging and existing propulsion technologies. This would decrease the roundtrip duration to 195-days (120 days from Earth to Mars, a 14-day stay and a 75-day return) and, therefore, reduce the neutron induced dose equivalent to 6 ± 2 mSv/day.

Acknowledgements

RAD is supported by NASA (HEOMD) under JPL subcontract #1273039 to Southwest Research Institute and in Germany by DLR and DLR's Space Administration grant numbers 50QM0501 and 50QM1201 to the Christian Albrechts University, Kiel. Part of this research was carried out at the Jet Propulsion Laboratory, California Institute of Technology, under a contract with the National Aeronautics and Space Administration. The data used in this paper are archived in the NASA Planetary Data System's Planetary Plasma Interactions Node at the University of California, Los Angeles. The archival volume includes the full binary raw data files, detailed descriptions of the structures therein, and higher-level data products in human-readable form. The PPI node is hosted at the following URL: http://ppi.pds.nasa.gov/.

References

Agostinelli, S., Allison, J., Amako, K., Apostolakis, J., Araujo, H., Arce, P., Asai, M., Axen, D., Banerjee, S., Barrand, G., Behner, F., Bellagamba, L., Boudreau, J., Broglia, L., Brunengo, A., Burkhardt, H., Chauvie, S., Chuma, J., Chytracek, R., Cooperman, G., Cosmo, G., Degtyarenko, P., Dell'Acqua, A., Depaola, G., Dietrich, D., Enami, R., Feliciello, A., Ferguson, C., Fesefeldt, H., Folger, G., Foppiano, F., Forti, A., Garelli, S., Giani, S., Giannitrapani, R., Gibin, D., Gómez Cadenas, J., González, I., Gracia Abril, G., Greeniaus, G., Greiner, W., Grichine, V., Grossheim, A., Guatelli, S., Gumplinger, P., Hamatsu, R., Hashimoto, K., Hasui, H., Heikkinen, A., Howard, A., Ivanchenko, V.N., Johnson, A., Jones, F., Kallenbach, J., Kanaya, N., Kawabata, M., Kawabata, Y., Kawaguti, M., Kelner, S., Kent, P., Kimura, A., Kodama, T., Kokoulin, R., Kossov, M., Kurashige, H., Lamanna, E., Lampén, T., Lara, V., Lefebure, V., Lei, F., Liendl, M., Lockman, W., Longo, F., Magni, S., Maire, M., Medernach, E., Minamimoto, K., Mora de Freitas, P., Morita, Y., Murakami, K., Nagamatu, M., Nartallo, R., Nieminen, P., Nishimura, T., Ohtsubo, K., Okamura, M., O'Neale, S., Oohata, Y., Paech, K., Perl, J., Pfeiffer, A., Pia, M., Ranjard, F., Rybin, A., Sadilov, S., Dic Salvo, E., Santin, G., Sasaki, T., Savvas, N., Sawada, Y., Scherer, S., Sei, S., Sirotenko, V., Smith, D., Starkov, N., Stoecker, H., Sulkimo, J., Takahata, M., Tanaka, S., Tcherniaev, E., Safai Tehrani, E., Tropeano, M., Truscott, P., Uno, H., Urban, L., Urban, P., Verderi, M., Walkden, A., Wander, W., Weber, H., Wellisch, J., Wenaus, T., Williams, D., Wright, D., Yamada, T., Yoshida, H., Zschiesche, D., 2003. Geant4—a simulation toolkit. Nucl. Instrum. Methods Phys. Res., Sect. A, Accel. Spectrom. Detect. Assoc. Equip. 506 (3), 250–303.

Drake, B.G., Hoffman, S.J., Beaty, D.W., 2010. Human exploration of Mars, Design Reference Architecture 5.0. In: 2010 IEEE Aerosp. Conf. IEEE, pp. 1–24.

Durante, M., Cucinotta, F.A., 2011. Physical basis of radiation protection in space travel. Rev. Mod. Phys. 83 (4), 1245–1281.

Ehresmann, B., Zeitlin, C., Hassler, D.M., Wimmer-Schweingruber, R.F., Böhm, E., Böttcher, S., Brinza, D.E., Burmeister, S., Guo, J., Köhler, J., Martin, C., Posner, A., Rafkin, S., Reitz, G., 2014. Charged particle spectra obtained with the Mars Science Laboratory Radiation Assessment Detector (MSL/RAD) on the surface of Mars. J. Geophys. Res., Planets 119 (3), 468–479.

Feldman, W.C., Lawrence, D.J., Goldsten, J.O., Gold, R.E., Baker, D.N., Haggerty, D.K., Ho, G.C., Krucker, S., Lin, R.P., Mewaldt, R.A., Murphy, R.J., Nittler, L.R., Rhodes, E.A., Slavin, J.A., Solomon, S.C., Starr, R.D., Vilas, F., Vourlidas, A., 2010. Evidence for extended acceleration of solar flare ions from 18 MeV solar neutrons detected with the MESSENGER Neutron Spectrometer. J. Geophys. Res. 115 (A1), A01102.

Folta, D.C., Vaughn, F.J., Rawitscher, G.S., Westmeyer, P.A., 2012. Fast Mars transfers through on-orbit staging. LPI Contrib. 1679.

Hassler, D.M., Zeitlin, C., Wimmer-Schweingruber, R.F., Böttcher, S., Martin, C., Andrews, J., Böhm, E., Brinza, D.E., Bullock, M.A., Burmeister, S., Ehresmann, B., Epperly, M., Grinspoon, D., Köhler, J., Kortmann, O., Neal, K., Peterson, J., Posner, A., Rafkin, S., Seimetz, L., Smith, K.D., Tyler, Y., Weigle, G., Reitz, G., Cucinotta, F.A., 2012. The Radiation Assessment Detector (RAD) investigation. Space Sci. Rev. 170 (1–4), 60.

Hassler, D.M., Zeitlin, C., Wimmer-Schweingruber, R.F., Ehresmann, B., Rafkin, S., Eigenbrode, J.L., Brinza, D.E., Weigle, G., Böttcher, S., Böhm, E., Burmeister, S., Guo, J., Köhler, J., Martin, C., Reitz, G., Cucinotta, F.A., Kim, M.-H., Grinspoon, D., Bullock, M.A., Posner, A., Gómez-Elvira, J., Vasavada, A.R., Grotzinger, J.P., 2014. Mars' surface radiation environment measured with the Mars Science Laboratory's Curiosity rover. Science 343, 1244797.

Hess, W., Patterson, H., Wallace, R., Chupp, E., 1959. Cosmic-ray neutron energy spectrum. Phys. Rev. 116 (2), 445–457.

Hohmann, W., 1994. Die Erreichbarkeit der Himmelskörper. Untersuchungen über das Raumfahrtproblem. Oldenbourg, München, Germany.

Ivanchenko, V.N., 2004. Geant4: physics potential for instrumentation in space and medicine. Nucl. Instrum. Methods Phys. Res., Sect. A, Accel. Spectrom. Detect. Assoc. Equip. 525 (1), 402–405.

Köhler, J., 2012. Gamma/neutron separation in the Martian radiation environment Dissertation. Ph.D. thesis. Christian-Albrechts-Universität zu Kiel.

Köhler, J., Ehresmann, B., Martin, C., Böhm, E., Kharytonov, A., Kortmann, O., Zeitlin, C., Hassler, D.M., Wimmer-Schweingruber, R., 2011. Inversion of neutron/gamma spectra from scintillator measurements. Nucl. Instrum. Methods Phys. Res., Sect. B, Beam Interact. Mater. Atoms 269 (22), 2641–2648.

Köhler, J., Zeitlin, C., Ehresmann, B., Wimmer-Schweingruber, R.F., Hassler, D.M., Reitz, G., Brinza, D.E., Weigle, G., Appel, J., Böttcher, S., Böhm, E., Burmeister, S., Guo, J., Martin, C., Posner, A., Rafkin, S., Kortmann, O., 2014. Measurements of the neutron spectrum on the Martian surface with MSL/RAD. J. Geophys. Res., Planets 119 (3), 594–603.

Koning, A.J., 2007. New working methods for nuclear data evaluation: how to make a nuclear data library? In: Int. Conf. Nucl. Data Sci. Technol. EDP Sciences, Les Ulis, France, pp. 679–684.

Press, W., 2007. Numerical Recipes: The Art of Scientific Computing. Cambridge University Press.

Share, G.H., Murphy, R.J., Tylka, A.J., Kozlovsky, B., Ryan, J.M., Gwon, C., 2011. Physics of solar neutron production: questionable detection of neutrons from the 31 December 2007 flare. J. Geophys. Res. 116 (A3), A03102.

Simonsen, L.C., Wilson, J.W., Kim, M.H., Cucinotta, F.A., 2000. Radiation exposure for human Mars exploration. Health Phys. 79 (5), 515–525.

United States Nuclear Regulatory Comission, 2009. Code of Federal Regulations, 10 CFR 20.1004. Tech. rep. United States Nuclear Regulatory Comission.

Zeitlin, C., Hassler, D.M., Cucinotta, F.A., Ehresmann, B., Wimmer-Schweingruber, R.F., Brinza, D.E., Kang, S., Weigle, G., Bottcher, S., Bohm, E., Burmeister, S., Guo, J., Köhler, J., Martin, C., Posner, A., Rafkin, S., Reitz, G., 2013. Measurements of energetic particle radiation in transit to Mars on the Mars Science Laboratory. Science 340 (6136), 1080–1084.